Wireless Portable Evaluation Platform for Photodynamic Therapy: *In vitro* Assays on Human Gastric Adenocarcinoma Cells

Rodrigo Henrique Gounella, Ilaiáli Souza Leite, Natalia Mayumi Inada, and João Paulo Carmo

***Abstract*—Photodynamic Therapy (PDT) is a technique used in the selective destruction of cancer cells and requires the previous knowledge of light dosimetry and photosensitizer drug (PS) concentration to apply on cells. Therefore, a laboratory platform is required for further evaluation, e.g. to make evaluation and assays on previously collected cells by biopsy to determine the best combination of light dose and PS concentration. In this context, this paper presents a low-cost, low-sized and flexible Wireless Portable Evaluation Platform for PDT assays on cells. The W-PEP was tested and evaluated using assays with Human Gastric Adenocarcinoma (AGS) cells. The AGS cells were exposed to the 5-aminolevulinic acid (ALA), which is a precursor of the photosensitive agent Protoporphyrin IX (PpIX) with absorption at 635nm. The W-PEP is composed by 16 small-sized LEDs matrix with peak transmittance at 634nm mounted in a PCB and controlled by ESP32-DevKitC®, a power bank to supply the lighting and the controlling systems and 3D printed components specially designed to allow portability and PDT assays. A graphical user interface (GUI) application for mobile devices was developed allowing the bi-directional communication between the smartphone and W-PEP via Bluetooth. The measurements with AGS cells proved this W-PEP was effective in its purpose and promoted cell death in samples treated with ALA and a final light dose of 5J/cm^2 after 49 minutes of light exposure. This W-PEP has 140mm of both length and width, 75mm of height and costs about $82.10. To finish, this system checks the optimal conditions that will be applied in the treatment after, thereby decreasing the costs and time of the application.**

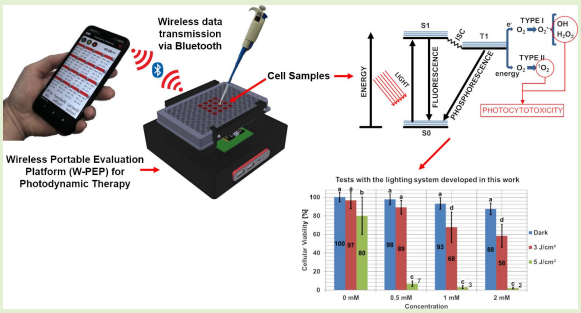

***Index Terms*— Photodynamic therapy (PDT), 5-Aminolevulinic Acid (ALA), Internet of Things (IoT), Android Application, Adenocarcinoma Gastric of Stomach (AGS).**

I. Introduction

ACCORDING to World Health Organization and World Cancer Research Fund, cancer can be considered as one of the major health problems around the World. There were an estimated 18 million cancer cases around the world in a year and is the second leading cause of death globally. About 1 in 6 deaths is due to cancer. Stomach cancer is between the 5 most incidents cases and is one of the most dangerous, because is the third in death causes [1], [2]. It is important to discover the cancer early, because the chance of reversing increases exponentially [1].

There is a lot of research in identifying Volatile Organic Compounds to find cancer in its early stages. For this purpose, mass spectrometry techniques [3], array of sensors [4], electrochemical sensors [5], microwave sensors [6], optical fiber sensor [7] have been used.

After the cancer is identified and located, a non-invasive treatment, called Photodynamic Therapy (PDT), can be performed. PDT is an optical technique that consists on an ablative treatment for rapidly proliferating abnormalities including dysplastic and malignant lesions. It is based on Photosensitizer Drug (PS) administration followed by exposure to a light with specific wavelength λ [nm], commonly located in the red region of the visible spectrum, due deeper penetration in biological tissue. After a certain time, the drug accumulates in lesions and the application of light with specific intensity and wavelength leads to it photoexcitation. PDT is a non-invasive therapy because the irradiation is limited to the tumor site, and at the same time, it presents low systemic toxicity and tumors selective destruction due to preferential buildup of the PS in injured tissues [8], [9]. Fig. 1 illustrates the basic principles of PDT.

Considering this regard, it is necessary to know before treatment starting which PS will be used, the concentration of this PS that will be prepared and the light dose that will

AQ:1 Manuscript received January 9, 2020; accepted January 30, 2020. The associate editor coordinating the review of this article and approving it for publication was Prof. Yu-Cheng Lin. *(Corresponding author: Rodrigo Henrique Gounella.)*

Rodrigo Henrique Gounella and João Paulo Carmo are with the Department of Electrical Engineering (SEL), University of São Paulo (USP), São Carlos 13566 590, Brazil (e-mail: rodrigogounella@usp.br).

Ilaiáli Souza Leite and Natalia Mayumi Inada are with the Group of Optics, São Carlos Institute of Physics (IFSC), University of São Paulo (USP), São Carlos 13566 590, Brazil.

Digital Object Identifier 10.1109/JSEN.2020.2971444

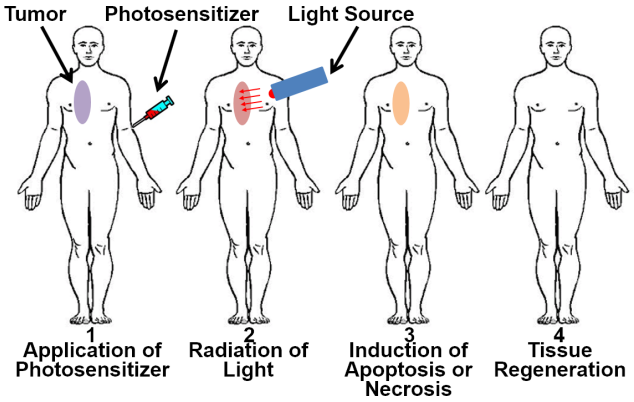

Fig. 1. Basic principles of PDT.

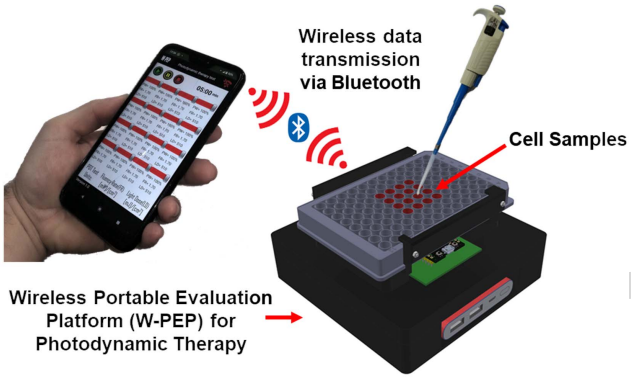

Fig. 2. Diagram of the W-PEP proposed in this paper.

be applied [10]–[13]. Thereby, it's possible to avoid patient unnecessary discomforts caused by the treatment and prevent the non-cancerogenous cells damages. Currently, there is a gap in portable photodynamic therapy (PDT) analysis systems that are flexible, portable with low-size and easy to interface with the operator.

In this context, using the concepts of IoT (Internet of things) and Android Application, this paper presents a Wireless Portable Evaluation Platform (W-PEP) controlled by a smartphone via Bluetooth connection (with the possibility to use Wi-Fi), which was specifically developed to perform and sensing PDT in Human Gastric Adenocarcinoma (AGS) cells submitted to 5-aminolevulinic acid (ALA) samples, a precursor of Protoporphyrin IX (PpIX).

II. Concept and Approach

A. Concept

This paper core is the development of a low-cost, low-sized and flexible Wireless Portable Evaluation Platform (W-PEP) that can assist and improve a cancer treatment by photodynamic therapy. The W-PEP performs a previous PDT in assays with cancerogenous cells before collected with a biopsy. Therefore, it's possible to check the optimal dosimetry and PS concentration that will be applied in the treatment after, decreasing the costs and time of the application.

Fig. 2 presents the W-PEP system overview controlled by a smartphone containing a 96-well microplate to irradiate the cells sample. The W-PEP control is done in real time by the graphical user interface (GUI) for mobile devices developed to simplify the operation for the end user. Additionally, this system was designed with a rechargeable power bank allowing totally portability.

The PDT module is composed by a high-performance microcontroller with wireless transceiver via Wi-Fi or Bluetooth, a power unit and a developed lighting system. The power unit comprises a power bank with rechargeable battery and the charging control system. There are many communication protocols for mobile devices, e g., IEEE 804.15.4, ZigBee, Wi-Fi, LTE, 3G and Bluetooth [14]. The last was chosen because it presents itself as a simple, low-cost and low-power consumption path to transmission and reception data and is present in almost all mobile devices [15], [16].

B. Photodynamic Therapy

The PDT principle involves the PS activation by specific light wavelength [9]. There are three main elements required: light, PS and oxygen. When the PS is exposed to a specific light wavelength, it is activated to an excited state. In the ground state (S0), it is said that a PS is in the singlet state, whereby all its electrons have paired spins in low energy orbitals. After applying light with a wavelength within the PS absorption band, the electron in the highest occupied molecular orbital (HOMO) is excited to the lowest unoccupied molecular orbital (LUMO). This process results in PS unstable singlet excited state (S1), which has nanosecond scale life time, and without any expected photodynamic activity. By referring to an unstable configuration, several processes can occur rapidly and the PS returns to its original state S0 by different processes, for example, by heat generation, a non-radioactive process, resulted from energy dissipation absorbed into the neighborhood molecules or by fluorescence, which is a photon emission with wavelength corresponding to the difference between two states energies [17]–[20].

Another possible process is the excited electron spin reversion, known as Intersystem Crossing (ISC). This process causes the PS to go into a lower energy excited state called triplet, which is relatively more stable than the singlet state. T1 has a micro to milliseconds scale life time, substantially larger than the S1 species and, therefore, is more prone to participate in photodynamic reactions, thus being the most critical process for PDT. At this point the molecule may undergo another excited electron spin reversion and return to the ground state by phosphorescence process, or it may interact with molecules in the medium. In the electronic transitions, triplet-triplet interactions are allowed by selection rules related to the multiplicity of spins, which allows the PS to interact with molecular oxygen that presents the triplet form in its ground state (O_2) [17]–[20].

The PDT oxidant characteristics discussion is centered on molecular oxygen (O_2). When the PS is in long-lived triplet state, it can interact with O_2 of two different ways. The Type I process occurs when the PS directly transfers an electron to O_2, producing superoxide anion ($O_2^{\cdot-}$), which can continue to form others reactive oxygen species (ROS) including the hydroxyl radical ($^{\cdot}OH$) and hydrogen peroxide (H_2O_2).

TABLE I
MAIN CHARACTERISTICS OF SOME PHOTOSENSITIZERS AVAILABLE COMMERCIALLY OR IN CLINICAL TESTS [18], [22]–[24]

Commercial name	λ [nm]	φ_Δ	ε [$M^{-1}.cm^{-1}$]	Class	Compound	Remarks
Photofrin®	632	0.89	3000	Porphyrins	*Porfimer sodium*	Commercial
Levulan®	635	0.56	5000	Porphyrins	*5-Aminolevulinic acid* (ALA)	
Foscan®	652	0.87	35000	Chlorines	*Meta-tetra(hydroxyphenyl)chlorin* (m-THPC)	Clinical tests
Photochlor®	665	0.48	47000	Feoforbides	*2-(1-Hexyloxyethyl)-2-devinyl pyropheophorbide* (HPPH)	
Laserphyrin®	664	0.77	40000	Chlorines	*N-aspartyl chlorin e6* (NPe6)	
Visudyne®	689	0.84	34000	Porphyrins	*Benzoporphyrin derivative monoacid ring A* (BPD-MA)	Commercial
Purlytin®	664	0.70	30000	Chlorines	*Tin ethyl etiopurpurin*	Clinical tests
Lutrin®	732	0.11	42000	Texaphirine	*Motexafin lutetium* (Lu-Tex)	
Tookad®	763	0.50	88000	Feoforbides	*Palladium bacteriopheophorbide* (WST09)	
Photosens®	676	0.38	200000	Phthalocyanine	*Aluminum phthalocyanine tetrasulfonate* (AlPcS4)	

φ_Δ: Quantum yield of $^1O_2$
ε: Molar extinction coefficient

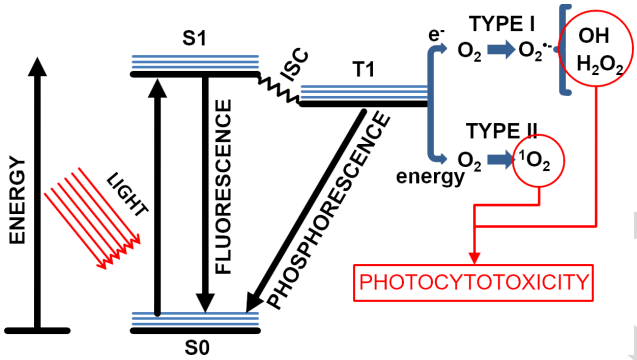

Fig. 3. Jablonski diagram showing the mechanisms involved in the photodynamic action, with the generation of excited states and reactive oxygen species (ROS).

Alternatively, the Type II process happens when there is energy transfer from PS in T1 state to O_2, resulting in the external electron spin inversion and creates a completely unoccupied orbital (a violation of Hund's rule). This type of oxygen is named singlet oxygen ($^1O_2$) with a short life time and is extremely reactive due its instable electronic configuration. Therefore, it effectively oxidizes many types of biomolecules (e.g., lipids, nucleic acids, etc.), which can lead to cell death and tissue destruction [17]–[20]. Fig. 3 presents a schematic of the processes involved in the "photodynamic action", known as Jablonski diagram.

C. Photosensitizer Drugs

There are many types of photosensitizing drugs available for use in PDT. Depending on the type of agent, they can be injected intravenously, ingested orally or applied topically [21]. Table I presents the main characteristics of some commercially available or undergoing clinical tests PSs.

Only three of the PSs presented in the Table I were approved by the Food and Drug Administration (FDA), Photofrin®, Levulan® and Visudyne®. The main compound of Levulan® is 5-aminolevulinic acid (ALA) that was approved by the FDA to treatment via PDT in 1999 [22]. ALA can be formulated for topical, oral or intravenous application [23].

ALA is a second-generation photosensitizer and a natural precursor of Protoporphyrin IX (PpIX) [24]–[26]. It is a photodynamically inactive, non-selective, non-toxic compound and is metabolized intracellularly to PpIX, which is photodynamically active. Subsequent illumination of the tumor site with red light activates the PpIX which causes oxidative damage and induces cytotoxicity [18], [26].

After a successful preliminary study of skin tumors treatment, the use of this PS achieved worldwide success. Actinic keratosis and superficial basal cell lesions can be eliminated via PDT with ALA and, in several studies, photodynamic treatment with ALA has been shown to be highly effective compared to other dermatological procedures to eliminate early stage superficial non-melanoma cutaneous tumors [23]. ALA has also been used successfully for head and neck tumors, Barrett's esophagus, urinary bladder, uterus and even prostate cancer [18], [23], [26], showing great potential to treat many types of cancerous pathologies.

The ALA's bioactivation utilizes the heme biosynthesis pathway enzymatic machinery. Although almost all types of human cells contain the enzymes involved in heme synthesis, a distinct activity of enzymes in tumors compared to unaffected tissues leads to increased accumulation of PpIX within tumor cells [25].

Considering the qualities and advantages of ALA, this photosensitizer was chosen to be used in this work.

D. Dosimetry

As previously mentioned, clinical PDT involves a PS application followed by illumination with appropriate wavelength and intensity to activate it. Ideally, this will result in an ablative photodynamic reaction that eliminates the lesion but spares normal tissue [27].

Before the required light dose (LD) quantification to activate a PS, it is necessary to first measure the fluency rate FR, which represents the optical power P_0 [W], in each area unit corresponding to the abnormal tissue A_{AT} [m^2] [23]. The fluency rate is given by:

$$FR = P_0 / A_{AT} \quad (1)$$

By determining the time interval Δt [s] at which the fluency rate is applied, the desired light dose is then calculated as follows [23]:

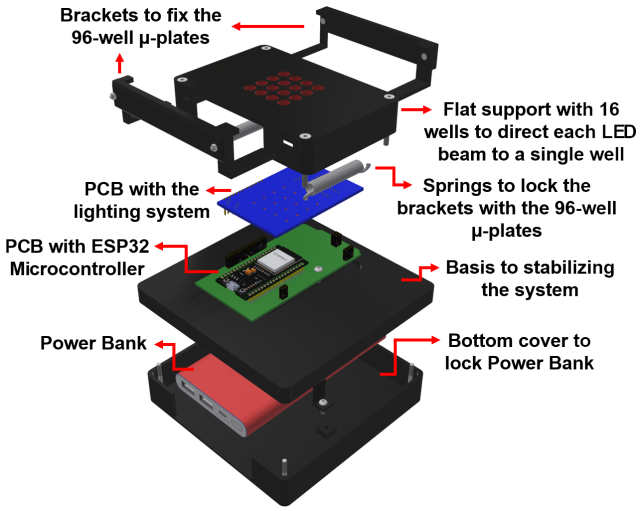

Fig. 4. 3D drawing for the assembled Wireless Portable Evaluation Platform (W-PEP).

$$LD = (P_0/A_{AT}) \times \Delta t \quad (2)$$

The light dose is a very important parameter, taking into account that it is a crucial factor for the PS activation, which, consequently, will result in abnormal tissue elimination. Unfortunately, no real-time dosimetry system exists, since it is very difficult to predict the light beam behavior interacting with a determined tissue. This happens because biological tissues are considered as turbid media, that is, they have high light absorption and dispersion rates. Then, when a beam interacts with a tissue, it has its intensity deteriorated as it penetrates due to the strong absorption and dispersion. In this way, the definition of necessary light doses for the treatment in diverse pathologies is determined based on results of clinical tests and in medical literature [28]–[30].

Thus, the system developed and showed in this paper, can minimize unnecessary time and cost expenses which are precious and crucial quantities in clinical applications.

III. Design

A. 3D Prototype of the W-PEP

The designed and assembled W-PEP first component was the developed Printed Circuit Boards (PCBs) with ESP32 and matrix of 16 LEDs. The distance between each LED was based on the standard measurements of 96-well microplates for cell culture, so that, each LED illuminates a single well. To supply the electronic components, a rechargeable power bank with 30000mAh was used. Fig. 4 presents a tri-dimensional (3D) model built in Computer Aided Design (CAD) software. The module supports were entirely printed by a 3D printer model GTMax®3D Core A1, using an ABS (acrylonitrile butadiene styrene) filament with 1.75mm in diameter and black color to not interfere in the analysis. The final dimensions of the entire module are 140 × 140 × 75 [mm^3].

B. Light Source Selection

Light sources are separated into two types, Laser and Non-Laser. Laser types include Argon Lasers, Dye Lasers, Metal Vapor Lasers, Diode Lasers and Neodymium-doped and Tritium Aluminum Garnet (Nd: YAG). Non-Laser types include LEDs, quartz halogen lamps with tungsten filaments, xenon lamps, metal halide lamps, phosphor-coated sodium lamps and fluorescent lamps [21], [30].

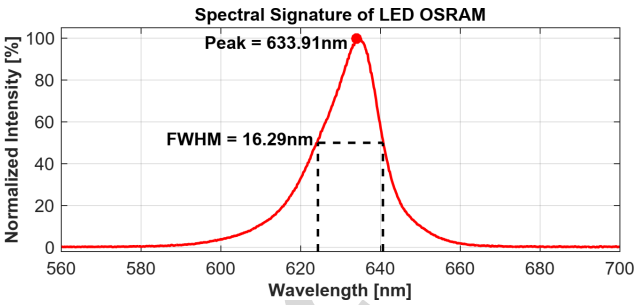

Fig. 5. Spectral signature of the LED LRQ396-P1Q2-1.

Laser type sources are widely used in PDT, they can produce a beam with high optical power and very low spectral width, but they are expensive and require large equipment and a lot of energy. LEDs, on the contrary of Lasers, produce smaller optical power and higher FWHM (Full width at half maximum) but, in most cases, they are low-cost components, have very small dimensions and consume small amounts of energy. In order to choose the light source, all these parameters and the emission spectrum were considered, which should be in the red region of the visible spectrum with the maximum spectral emission around 635nm, to match the endogenous PpIX absorption produced by the selected compound, ALA.

Therefore, the selected light source was the LED, model LRQ396-P1Q2-1 [31] from Osram Opto Semiconductors, with small dimensions. This LED has the SMT 0603 component encapsulation standard and it has a height of 0.4 mm. Fig. 5 shows the spectral signature of the LED, which was measured with a spectrophotometer model USB4000 from Ocean Optics. It is also possible to observe in Fig. 5, the LED presents a spectral emission peak located at ≈ 634nm, a FWHM (full width at half maximum) of 16.29nm, confirming that this LED is an adequate light source for ALA-mediated PDT.

C. Hardware and Power Consumption

To achieve maximum power without damaging the LEDs, it was verified in the datasheet [31] the maximum forward current and voltage supported by these components and the values found were 2.3V of voltage and 20mA of current. The lighting control was performed by an ESP32-DevKitC® from Espressif and each LED was connected to a digital output which provides 3.19V. Considering these maximum values of voltage, current and the output voltage of ESP32-DevKitC® digital pin, the lighting system PCB was built containing 43Ω precision resistors with a tolerance 1%. This value of resistance was chosen because it is the commercial value closer to the required.

Fig. 6 shows the W-PEP electronic schematic. There are 16 LEDs in the W-PEP and each LED is connected to a single GPIO (general-purpose input/output) pin in the ESP32-DevKitC®. The LED PWM controller can generate

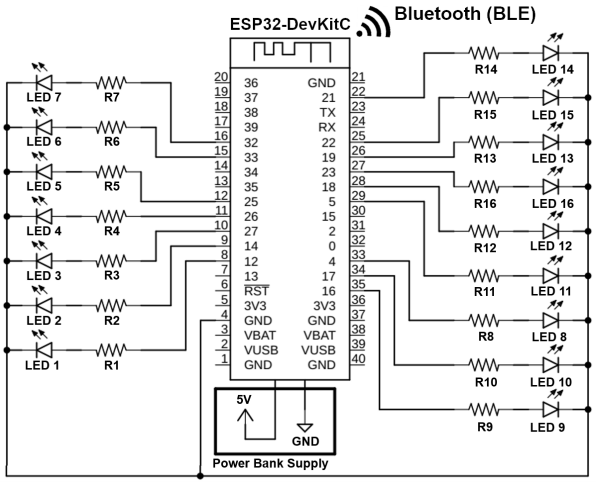

Fig. 6. Schematic diagram of the electronic circuit designed for the W-PEP.

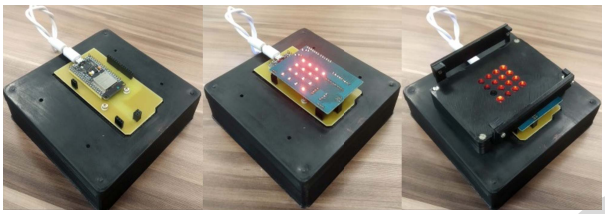

Fig. 7. Final developed W-PEP. (a) Just ESP32-DevKitC® Control unit, (b) All electronic components mounted and (c) W-PEP completely assembled.

16 independent channels of digital waveforms with configurable periods and duties. The 16 channels of digital waveforms operate with an APB (Advanced Peripheral Bus) clock of 80MHz. Eight of these channels have the option of using the 8MHz oscillator clock. Each channel can select a 20-bit timer with configurable counting range, while its accuracy of duty can be up to 16 bits within a 1ms period.

The Bluetooth stack of ESP32® is compliant with the Bluetooth v4.2 BR/EDR (Basic Rate/Enhanced Data Rate) and BLE (Bluetooth low energy) specifications. BLE is the ideal for Internet of Things (IoT), therefore, it is the protocol has been used in this work.

All of electronic circuit of the W-PEP was fabricated on a fiberglass (FR-4) substrate by a mechanical prototyping machine model S103 form LPKF Laser & Electronics. Fig. 7(a) and (b) shows the W-PEP Hardware without the lighting system and with the lighting system, respectively. Fig. 7(c) shows all components of W-PEP assembled.

The consumption required to operate the W-PEP was determined experimentally as 420mA just receiving via Bluetooth and 550mA with Bluetooth transmitting as well under a voltage supply of 5V delivered by the power bank. The power bank used in the system has a 30000mAh capacity allowing a maximum of 54 hours autonomy.

D. Interface With Smartphone

The software was developed in C++ language to perform the communication between the mobile device and W-PEP.

A graphical user interface (GUI) application for mobile devices with real-time control and visualization parameters

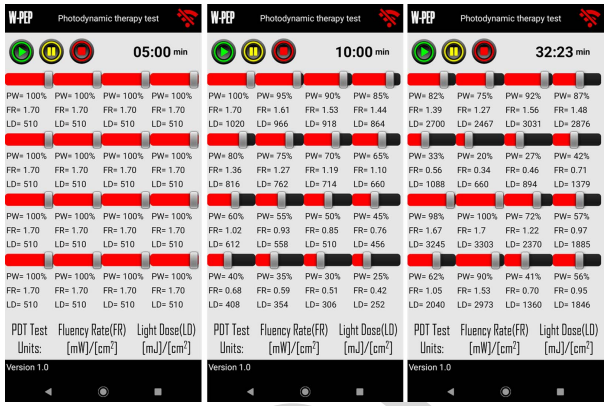

Fig. 8. App interface with different times and potencies delivered to the LEDs. (a) to 5 minutes, (b) to 10 minutes and (c) 32 minutes and 23 seconds.

TABLE II
ESTIMATED COST OF W-PEP

Component	Estimated Price (USD)
ESP32-DevKitC®	$8.45
FR-4 (15cm × 20 cm)	$2.56
16 LEDs LRQ396-P1Q2-1	$5.44
16 Resistors 43Ω 1% tolerance	$4.64
Power Bank 3000mAh	$26.99
ABS Cases and Supports	$34.02
Total	$82.10

was developed using MIT App Inventor, and a bidirectional communication protocol by Bluetooth was established for the data transmission and the real-time counters on the smartphone screen as shown in Fig. 8, where it is possible to observe the 16 sliders to control the power delivered for the LEDs from the selected 16 GPIOs ports of ESP32-DevKitC®, the chronometer to count the analysis time, the buttons to start, pause and stop/reset the timer and the indicators to show the values of potency delivered to each LED, Fluency Rate of each LED and the light dose delivered to each microplate well from each LED.

E. Estimated Cost and Comparison

The estimated cost of W-PEP is shown in Table II where is possible to observe the discrimination of each main component that compound the lighting and communication system developed in this work.

There are others similar devices found in the literature [32]–[34] with the resemble objective presented in this work. The systems developed in [32] and [33] are composed by 70 LEDs in a 10 × 7 arrangement array and 96 LEDs in a 12 × 8 arrangement array, respectively. Both have the same dimensions with 30 × 20 × 31.5 [cm^3], that are much bigger than W-PEP, need air cooling to decrease the temperature, the LEDs are connected in series and use a lifting platform with 1mm adjustment to regulate the distance between the LEDs and microplates, but in [33] is used an electronic system controlled by software to adjust this distance and irradiation doses based on time and power. The arrangement in series entails some disadvantages, e. g., if one LED fails, the rest

fails too; the fluency rate of each LED is equal without the possibility of control this quantity in each LED individually.

In order to obtain different irradiances simultaneously, six optical attenuators were put onto the wells of the 96-well plate, as described in [32]. Already on W-PEP, it can be configured 16 real-time irradiances, because each LED is connected in an individual ESP32-DevKitC® GPIO with 16 bits resolution.

The light source system developed in [34] is composed by a custom-made planar array of 30 LEDs, an aluminum supporting structure with screws and holders built for positioning the light source and a black breadboard acting as a structure base. Therefore, as can be observed in [34], the light source structure is much more complex than W-PEP and, once again, there isn't individual control of each LED fluency rate.

None of these light source systems [32]–[34] can be considered portable because they are wired, have weighted structures and do not use microcontroller devices to control the fluency rate, light dose and perform PDT with real-time determination of these quantities. Just W-PEP is completely wireless and can be controlled remotely by portable devices, such as smartphone, and uses the concepts of IoT (Internet of things) and Android Application to perform PDT tests on cells.

IV. Results and Discussion

A. Cells Preparation for PDT and Evaluation of Endogenous Protoporphyrin Production

It was used in the experiments a cell line culture of Human Gastric Adenocarcinoma (AGS, catalog number BCRJ 0311), collected from the stomach of a 54-year-old female patient and acquired from Rio de Janeiro cell bank [34].

The next procedures with the cell samples were performed to verify the endogenous Protoporphyrin production mediated by ALA incubation. Therefore, it was possible to determine the optimal concentration of PS for this cell line.

The culture medium to maintain the cells was Dulbecco's modified Eagle Medium (DMEM) supplemented with 10% of fetal bovine serum (FBS) and glucose, providing the final concentration of 4.5g/L. The cells were cultured in 75cm^2 cell culture flasks from Greiner Bio One and kept in a humidified incubator, model MCO-17AC (Sanyo Electric Co. Ltd), at 37°C and atmosphere with 5% of carbon dioxide (CO_2).

The cells were dissociated from the culture flasks 24 hours prior to the experiments and 100μL of a 5×10^4 cells/mL suspension were seeded in 96-well microplates from Corning Inc. These microplates were kept in the incubator. After 24 hours, a 10mM stock solution was prepared with 5-Aminolevulinic Acid Hydrochloride (5-ALA) in phosphate buffered saline (PBS), and then filtered through a sterile syringe with 0.2μm cellulose acetate membrane filter (Corning Inc.).

The fluorescence evaluation of this compound was tracked using the fluorescence microscopy; model Axio Observer.Z1 from ZEISS, to observe the production of endogenous PpIX by AGS cells. The microscopy images were obtained by incubating a solution of 2mM ALA diluted in culture medium DMEM without phenol red and supplemented with 10% FBS for 1, 3, 8 and 24 hours. After the incubation, the cells were washed with PBS and fresh culture medium was added.

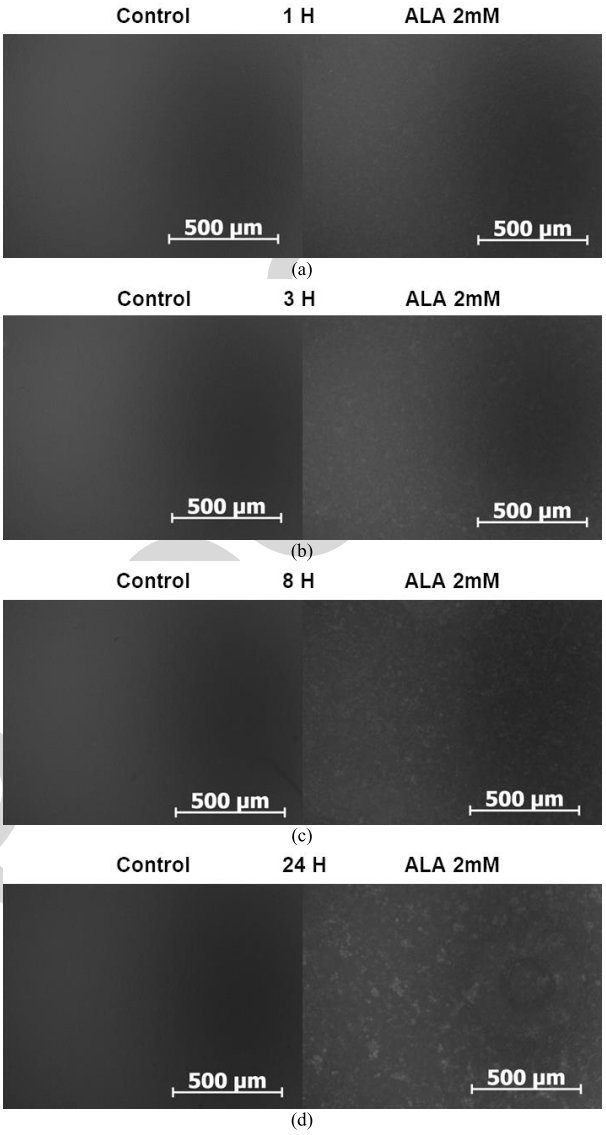

Fig. 9. Images obtained by fluorescence microscopy showing the production of PpIX. Photographs taken after (a) 1 hour, (b) 3 hours, (c) 8 hours, and (d) 24 hours.

As shown in Fig. 9(a) and (b), few differences were observed between the control group (not exposed to ALA) and the 2mM ALA group in the fluorescence images to 1 and 3 hours of incubation, respectively.

However, with 8 hours of incubation, shown in Fig. 9(c), it is possible to observe the presence of fluorescent regions in the group incubated with ALA, which becomes more evident after 24 hours of incubation, presented in Fig. 9(d). The observed contrast between the control group and incubated with the 2mM solution suggests the presence of PpIX at higher concentrations in samples exposed to ALA, indicating the increased photosensitizer accumulation inside the cells after the 24 hours interval.

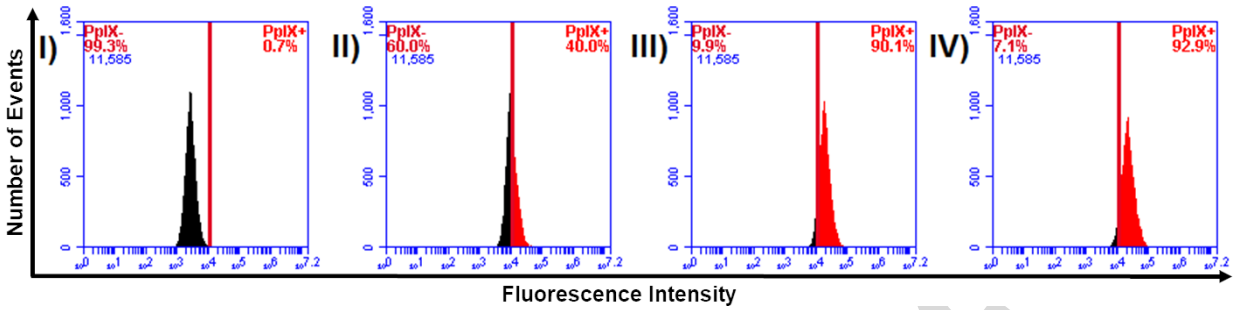

Fig. 10. Histograms of flow cytometry in the FL-3 channel. Groups: I) control, II) 0.5 mM ALA, III) 1 mM ALA and IV) 2 mM ALA. Cells exhibiting just autofluorescence (PpIX−) are marked in black, and cells showing high fluorescence of PpIX (PpIX+) are marked in red.

To confirm that the signal detected in the images corresponds to ALA – PpIX conversion, cells incubated with ALA for a 24 hours interval were evaluated by flow cytometry.

To analyze the influence in PpIX production of different ALA concentrations, solutions of 0.5, 1 and 2mM were incubated with AGS cells. The histogram of the control group (Fig. 10-I) shows the autofluorescence of the samples, allowing the delimitation of two fixed regions, one called PpIX−, which comprises the plot area with the samples autofluorescence, containing the fluorescence intensity of endogenous PpIX basal levels and other endogenous chromophores in the FL-3 channel (excitation: 488 nm; optical filter for fluorescence detection: 670 LP) in the cell population; and another called PpIX+, which contains the region with higher fluorescence intensities in the red region, thus containing cells with higher endogenous PpIX concentrations.

The cell incubation with 0.5 mM ALA solution (Fig. 10-II) resulted in a population migration to the region of higher fluorescence intensity, where 40% of cells produced PpIX. Higher concentrations of ALA resulted in migration from almost the entire population to the region of highest fluorescence intensity, indicating that approximately 90% of cells produced higher levels of photosensitizer. However, no large difference was observed between groups incubated with 1mM ALA solutions (Fig. 10-III) and 2mM (Fig. 10-IV), suggesting that the cells achieved their maximum efficiency of ALA to PpIX conversion when incubated for 24 hours with 1mM ALA.

B. Optical and Thermal Stability

In order to realize the PDT with this W-PEP, it is desirable that the maximum fluency rate provided by the selected LEDs be the same or at least with very close values. Therefore, with the assistance of the USB4000 spectrometer, the values of the maximum fluency rate of each 16 LEDs were measured and the mean value obtained was 1.7mW/cm^2 with a standard deviation of 0.06mW/cm^2 which shows small variation between measurements.

Other important quantity that affects the cell samples is the temperature. As the cells are provided by human stomach, it's is necessary to check the temperature rise caused by LEDs because when these values pass 37°C, the cells can begin to die due to overheating. So, with a thermal infrared camera the temperature of all microplate wells used in this work by W-PEP was measured for 90 minutes. Fig. 11 presents the results for these measurements with an interval of 10 minutes between each image.

It is possible to observe in Fig. 11 the increase of the used microplate wells temperature over time, but the temperature measured with 90 minutes of exposure is far below 37 Celsius degrees, which shows the system capacity to perform PDT for hours without causing cell death by the temperature.

C. PDT Activity

To evaluate the developed W-PEP three microplates were prepared and different concentrations of ALA (0.5, 1.0 and 2.0mM). The incubation time to allow cells to convert ALA in PpIX chosen was 24 hours, due the higher PpIX build up as showed in the Fig. 9(d).

After the ALA incubation, samples were washed twice with PBS and the supernatant was replaced by phenol-free DMEM supplemented with 10 FBS. Each plate received a different light dose and one remained protected from light (dark control). The chosen light doses were 3 and 5J/cm^2, which corresponded to 29 and 49 minutes of irradiation, respectively.

Just after irradiation, the microplates were transferred back to incubator and kept for 24 hours. After this incubation time the culture medium was then replaced with phenol-free DMEM supplemented with and 10% MTT (3-[4,5-Dimethylthiazol-2-yl]-2,5-Diphenyltetrazolium Bromide from Sigma-Aldrich and returned to the incubator for 3 hours.

Thereafter, the MTT solution was replaced with DMSO (Dimethylsulfoxide) and absorbance measurements at 570 and 690 nm were performed on a Multiskan GO spectrophotometer from Thermo Fisher Scientific. The second wavelength was performed to remove the absorbance value of the material in the microplate bottom. The absorbance value of the treated groups Abs_a was calculated as follows:

$$Abs_a = (Abs_{570\text{nm}} - Abs_{690\text{nm}}) - Abs_{\text{white}} \quad (3)$$

where $Abs_{570\text{nm}}$ and $Abs_{690\text{nm}}$ were the absorbance measurements at 570nm and 690nm, respectively, and the Abs_{white} was absorbance value of samples that were not incubated with MTT to remove inferences in the assays.

The viability value was calculated by taking the ratio between each absorbance value of the treated groups Abs_a and the mean absorbance value of the control group Abs_c that

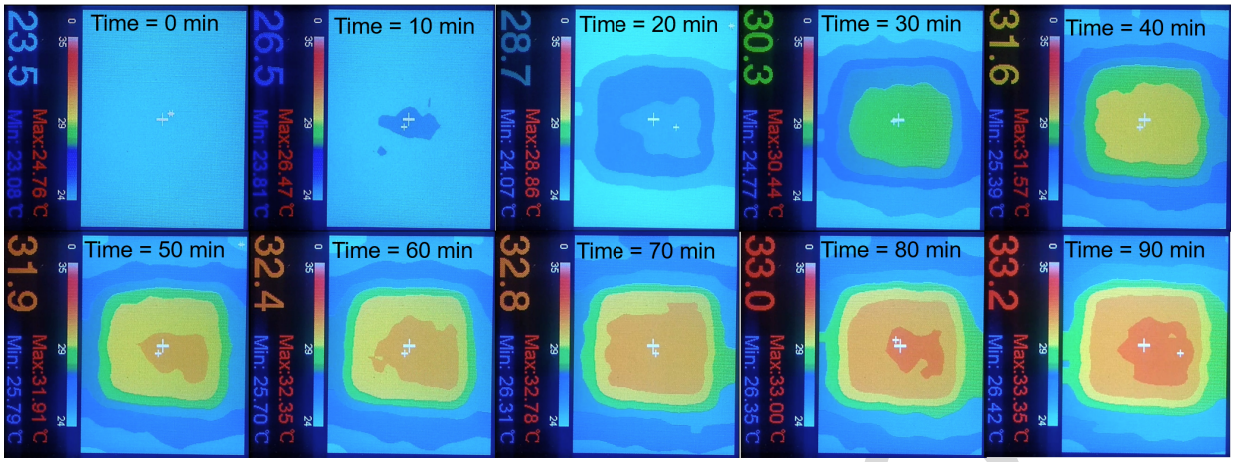

Fig. 11. Images collected from the thermal infrared camera every 10 minutes. The total time of measurements was 90 minutes and the temperature did not exceed 35 Celsius degrees.

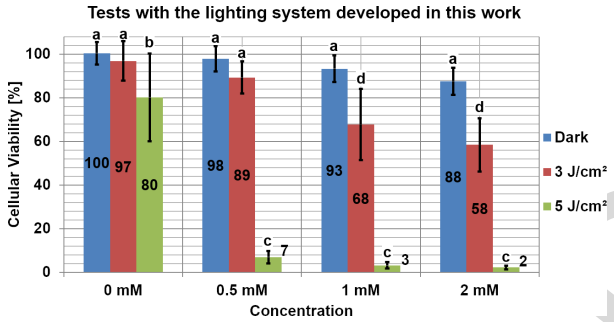

Fig. 12. Values (in %) of the tumor cell viability of the tumor cells from the control groups ("dark", bars in blue) corresponding to the cells treated or not with ALA and which did not were exposure to light and the treated groups, corresponding to the cells treated or not with ALA and irradiated with 3 (red) or 5 (green) J/cm^2.

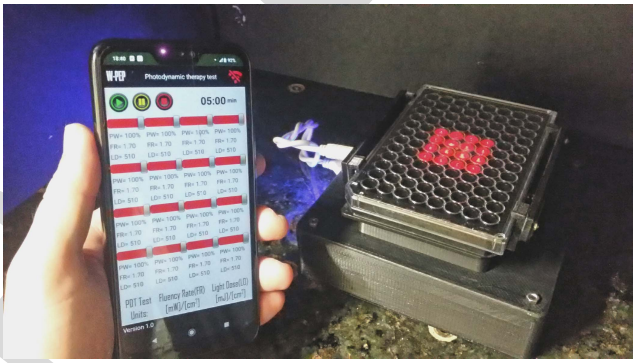

Fig. 13. Final prototype of the W-PEP side-by-side with its host smartphone.

was not exposed to ALA or to light, as described in equation (4).

$$Viability = (Abs_a/Abs_c) \times 100[\%] \quad (4)$$

The absorbance and viability values are expressed as the mean ± standard deviation. The experiments were performed with quadruplicate of each group, and were repeated in three different occasions. The GraphPad Prism 6 software was used to perform the statistical analysis of the results, using Analysis of Variance (ANOVA) followed by the Tukey multiple comparisons test. Statistically significant differences (represented by the letters a, b, c and d) were considered for the comparisons that presented a value of $p \leq 0.05$ (e.g., $p \leq 5\%$). The results are shown in Fig. 12.

As it can be observed in Fig. 12, ALA incubation alone did not affect samples viability. When exposed to light, samples incubated with ALA solutions of 0.5mM showed no change in cell viability when 3J/cm^2 were applied, but yielded 7% of viable cells after they were irradiated with 5J/cm^2. No further damage was observed by increasing the ALA concentration in samples exposed to the highest light dose resulting in 3% of viable cells with 1mM ALA solution and 2% with 2mM ALA solution. When exposed to 3J/cm^2, 1 and 2mM solutions displayed similar results, reducing cell viability to 68% and 58%, respectively. The absence of significant differences between groups incubated with 1 and 2mM solutions indicates a plateau is reached in the PpIX production with ALA 1mM. This hypothesis is corroborated by the flow cytometry histograms that display the same population shift towards higher fluorescence intensity in the FL-3 channel in PpIX.

V. Conclusion

A Wireless Portable Evaluation Platform (W-PEP) was successful developed and the proof of principles showed significant results by selectively killing Human Gastric Adenocarcinoma (AGS) cells by PDT at low fluencies rates. The portability of this photonic device, combined with its low-cost and large autonomy (about 54 hours) are promising to be used in a near future for assist the cancer treatments by Photodynamic Therapy decreasing the costs and time of the application, which is of utmost importance in these situations. It is also important to highlight the implementation of IoT concepts to improve medical diagnostics and equipment.

Fig. 13 shows a functional prototype of W-PEP side-by-side and connected with the smartphone running a host application.

References

[1] World Health Organization. *Cancer*. [Online]. Available: https://www.who.int/news-room/fact-sheets/detail/cancer
[2] World Cancer Research Fund. *Worldwide Cancer Data: Global Cancer Statistics for the Most Common Cancers*. [Online]. Available: https://www.wcrf.org/dietandcancer/cancer-trends/worldwide-cancer-data

AQ:2

[3] M. Woollam *et al.*, "Detection of volatile organic compounds (VOCs) in urine via gas chromatography-mass spectrometry QTOF to differentiate between localized and metastatic models of breast cancer," *Sci. Rep.*, vol. 9, Feb. 2019, Art. no. 2526.
[4] L. Zhao, X. Li, J. Wang, P. Yao, and S. A. Akbar, "Detection of formaldehyde in mixed VOCs gases using sensor array with neural networks," *IEEE Sensors J.*, vol. 16, no. 15, pp. 6081–6086, May 2016.
[5] Y. Zhang *et al.*, "Identification of volatile biomarkers of gastric cancer cells and ultrasensitive electrochemical detection based on sensing interface of Au-Ag alloy coated MWCNTs," *Theranostics*, vol. 4, no. 2, pp. 154–162, 2014.
[6] M. H. Zarifi, A. Sohrabi, P. M. Shaibani, M. Daneshmand, and T. Thundat, "Detection of volatile organic compounds using microwave sensors," *IEEE Sensors J.*, vol. 15, no. 1, pp. 248–254, Jan. 2015.
[7] S.-H. Yeom *et al.*, "VOCs detection based on evanescent wave coupling of dye-coated optical fiber," *IEEE Sensors J.*, vol. 15, no. 5, pp. 3021–3025, May 2015.
[8] B. T. Petersen *et al.*, "Photodynamic therapy for gastrointestinal disease," *Gastrointestinal Endoscopy*, vol. 63, no. 7, pp. 927–932, 2006.
[9] S. V. Kantsevoy *et al.*, "Endoscopic mucosal resection and endoscopic submucosal dissection," *Gastrointestinal Endoscopy*, vol. 68, no. 1, pp. 11–18, 2008.
[10] H. Liu *et al.*, "Development and evaluation of a low-cost, portable, LED-based device for PDT treatment of early-stage oral cancer in resource-limited settings," *Lasers Surg. Med.*, vol. 51, no. 4, pp. 345–351, Apr. 2019.
[11] A. Bansal, F. Yang, T. Xi, Y. Zhang, and J. S. Ho, "*In vivo* wireless photonic photodynamic therapy," *Proc. Nat. Acad. Sci. USA*, vol. 115, no. 7, pp. 1469–1474, Feb. 2018.
[12] J. Hempstead *et al.*, "Low-cost photodynamic therapy devices for global health settings characterization of battery-powered LED performance and smartphone imaging in 3D tumor models," *Sci. Rep.*, vol. 5, May 2015, Art. no. 10093.
[13] I. S. Leite, J. L. Vivero-Escoto, Z. Lyles, V. S. Bagnato, and M. Inada, "*In vitro* evaluation of photodynamic therapy using redox-responsive nanoparticles carrying PpIX," *Proc. SPIE*, vol. 10476, Mar. 2018, Art. no. 104760W.
[14] J. Carmo and J. Correia, "Wireless instrumentation," *Measurement, Instrumentation, and Sensors Handbook: Two-Volume Set*, J. G. Webster, Ed., 2nd ed. Boca Raton, FL, USA: CRC Press, 2014, pp. 1–25.
[15] K. A. Agha *et al.*, "Which wireless technology for industrial wireless sensor networks the development of OCARI technology," *IEEE Trans. Ind. Electron.*, vol. 56, no. 10, pp. 4266–4278, Oct. 2009.
[16] J. P. De Campos Da Costa, W. B. Bastos, P. I. Da Costa, M. A. Zaghete, E. Longo, and J. P. Carmo, "Portable laboratory platform with electrochemical biosensors for immunodiagnostic of hepatitis C virus," *IEEE Sensors J.*, vol. 19, no. 22, pp. 10701–10709, Nov. 2019.
[17] D. E. Dolmans, D. Fukumura, and R. K. Jain, "Photodynamic therapy for cancer," *Nature Rev. Cancer*, vol. 3, no. 5, pp. 380–387, 2003.
[18] S. Yano *et al.*, "Current states and future views in photodynamic therapy," *J. Photochem. Photobiol. C, Photochem. Rev.*, vol. 12, no. 1, pp. 46–67, Mar. 2011.
[19] M. Scholz and M. Didie, "New trends in photodynamic therapy research," in *Proc. WDS*, 2012, pp. 46–51.
[20] T. G. S. Denis *et al.*, "All you need is light: Antimicrobial photoinactivation as an evolving and emerging discovery strategy against infectious disease," *Virulence*, vol. 2, no. 6, pp. 509–520, Nov. 2011.
[21] D. Dave, U. Desai, and N. Despande, "Photodynamic therapy: A view through light," *J. Orofacial Res.*, vol. 2, pp. 82–86, Apr. 2012.
[22] A. Ormond and H. Freeman, "Dye sensitizers for photodynamic therapy," *Materials*, vol. 6, no. 3, pp. 817–840, Mar. 2013.
[23] R. R. Allison and C. H. Sibata, "Oncologic photodynamic therapy photosensitizers: A clinical review," *Photodiagnosis Photodyn. Therapy*, vol. 7, no. 2, pp. 61–75, Jun. 2010.
[24] C. M. N. Yow, C. K. Wong, Z. Huang, and R. J. Ho, "Study of the efficacy and mechanism of ALA-mediated photodynamic therapy on human hepatocellular carcinoma cell," *Liver Int.*, vol. 27, no. 2, pp. 201–208, Mar. 2007.
[25] M. Wachowska *et al.*, "Aminolevulinic acid (ALA) as a prodrug in photodynamic therapy of cancer," *Molecules*, vol. 16, no. 5, pp. 4140–4164, May 2011.
[26] Q. Peng *et al.*, "5-Aminolevulinic acid-based photodynamic therapy. Clinical research and future challenges," *Amer. Cancer Soc.*, vol. 79, no. 12, pp. 2282–2308, 1997.
[27] R. R. Allison and K. Moghissi, "Oncologic photodynamic therapy: Clinical strategies that modulate mechanisms of action," *Photodiagnosis Photodyn. Therapy*, vol. 10, no. 4, pp. 331–341, Dec. 2013.
[28] F. Fanjul-Vélez and J. L. Arce-Diego, "Light propagation in turbid media: Application to biological tissues," *Proc. 21st Int. Conf. Radio Elektronika*, 2011, pp. 7–10.
[29] R. R. Allison, G. H. Downie, R. Cuenca, X.-H. Hu, C. J. Childs, and C. H. Sibata, "Photosensitizers in clinical PDT," *Photodiagnosis Photodyn. Therapy*, vol. 1, no. 1, pp. 27–42, May 2004.
[30] I. Yoon, J. Z. Li, and Y. K. Shim, "Advance in photosensitizers and light delivery for photodynamic therapy," *Clin. Endoscopy*, vol. 46, no. 1, p. 7, 2013.
[31] *Osram Opto Semiconductors, Datasheet, LR Q396-P1Q2-1.* AQ:3
[32] D. Chen *et al.*, "Light-emitting diode-based illumination system for *in vitro* photodynamic therapy," *Int. J. Photoenergy*, vol. 2012, p. 6, Mar. 2012.
[33] Z. Jamali, S. M. Hejazi, S. M. Ebrahimi, H. Moradi-Sardareh, and M. Paknejad, "Effects of LED-based photodynamic therapy using red and blue lights, with natural hydrophobic photosensitizers on human glioma cell line," *Photodiagnosis Photodyn. Therapy*, vol. 21, pp. 50–54, Mar. 2018.
[34] J. A. Rodrigues, R. Amorim, M. F. Silva, F. Baltazar, R. F. Wolffenbuttel, and J. H. Correia, "Photodynamic therapy at low-light fluence rate: *In vitro* assays on colon cancer cells," *IEEE J. Sel. Topics Quantum Electron.*, vol. 25, no. 1, pp. 1–6, Jan. 2019.
[35] *Cell Bank of Rio de Janeiro, Datasheet, AGS (code 0311).*

Rodrigo Henrique Gounella was born in São Carlos, Brazil, in 1991. He graduated in physics engineering from UFSCar in 2016, and the M.Sc. degree in 2018 and conducts his Doctorate degree, both in electrical engineering with the Group of Metamaterials, Microwaves and Optics Telecommunications, USP, São Carlos, where he developed a system for photodynamic therapy. He is also a Mechanical Technician at SENAI Antonio Adolpho Lobbe in 2007.

Ilaiáli Souza Leite received the Diploma degree in physical and biomolecular sciences in 2013 and the M.Sc. degree in applied physics with biomolecular emphasis studying near-infrared photodynamic antimicrobial therapy from IFSC, USP, Brazil. She is currently pursuing the Ph.D. degree focusing on the optimization of photodynamic therapy for cancer treatment using nanostructured photosensitizers.

Natalia Mayumi Inada received the B.S. degree in pharmacy and the Ph.D. degree in medical pathophysiology from UNICAMP. She is currently a Researcher with USP, IFSC, leading the Microbial Control and Cell Culture Labs, Biophotonics Group, working on the development of clinical projects and implementing projects improving the photodynamic therapy with nanostructured photosensitizers.

João Paulo Carmo was born in Maia, Portugal, in 1970. He is a Professor with USP, São Carlos, Brazil, where he is also the Vice-Director of the Group of Metamaterials, Microwaves and Optics (GMeta). He is involved in the research on micro/nano-technologies for mixed-mode/RF and optic systems, solid-state integrated sensors, and microdevices for use in biomedical and industrial applications.